Geotech Geol Eng (2018) 36:531–549
https://doi.org/10.1007/s10706-017-0345-2

ORIGINAL PAPER

High Strain Rate Response of Rocks Under Dynamic Loading Using Split Hopkinson Pressure Bar

Sunita Mishra · Hemant Meena · Vedant Parashar · Anuradha Khetwal · Tanusree Chakraborty · Vasant Matsagar · Pradeep Chandel · Manjit Singh

Received: 18 January 2017 / Accepted: 18 August 2017 / Published online: 28 August 2017

Abstract In the present work, dynamic stress–strain response of five sedimentary and three metamorphic rocks from different regions of India, e.g. Kota sandstone, Dholpur sandstone, Kota limestone, Himalayan limestone, dolomite, quartzite, quartzitic gneiss and phyllite have been investigated through split Hopkinson pressure bar test at different strain rates. The dry density, specific gravity, static compressive strength and tensile strength values of the rocks have also been determined. Petrological studies of the rocks have been carried out through X-ray diffraction test and scanning electron microscope test. It is observed from the stress–strain response of the rocks that the peak stress increases with increasing strain rate. Dynamic increase factors for the strength of these rocks have been determined by comparing the dynamic and the static peak compressive stresses and correlation equations are proposed.

Keywords Dynamic increase factor · High strain rate · Metamorphic rock · Sedimentary rock · Split Hopkinson pressure bar

1 Introduction

In the twentieth century, manmade disasters, e.g. bomb blast, projectile attack, mine blast have created headlines in the news due to blast in London and Paris underground metro, projectile attack in Gaza, landmine blast in Kashmir. The disastrous events like blast or projectile attack, when happens underground, create a ground shock that gives rise to a high rate of loading of the soil and rock in the surroundings. Ngo et al. (2007) and Dusenberry (2010) mentioned that the strain rate generated in rock when subjected to blast

S. Mishra (✉) · H. Meena · V. Parashar · A. Khetwal · T. Chakraborty · V. Matsagar
Department of Civil Engineering, Indian Institute of Technology (IIT) Delhi, Hauz Khas, New Delhi 110 016, India
e-mail: sunita.mishra256@gmail.com

H. Meena
e-mail: hmnt24@gmail.com

V. Parashar
e-mail: vedantce@gmail.com

A. Khetwal
e-mail: anuradhasinha14@gmail.com

T. Chakraborty
e-mail: tanusree@civil.iitd.ac.in

V. Matsagar
e-mail: matsagar@civil.iitd.ac.in

P. Chandel · M. Singh
Terminal Ballistics Research Laboratory (TBRL), Defence Research and Development Organisation (DRDO), Sector - 30, Chandigarh 160 030, India
e-mail: pradeep.tbrl@gmail.com

M. Singh
e-mail: manjitsingh78@yahoo.com

loading may go as high as 10^2 to 10^4/s. The stress–strain response of rock, its peak stress, and stiffness are significantly affected when subjected to such high rate of loading (Blanton 1981; Li and Meng 2003). In the literature, different experimental techniques are available for characterization of materials under strain rate dependent loading as shown in Fig. 1 (Field et al. 2004). For the strain rate range induced by blast load as mentioned above, the split Hopkinson pressure bar (SHPB) technique may be adapted for characterization of geological materials.

The SHPB device was invented in 1949 by Kolsky (1949) and subsequently modified in 1953 by Kolsky (1953) for testing the dynamic properties of metals. In Civil Engineering practice, the SHPB tests were performed on various brittle materials such as concrete and ceramics (Ross et al. 1989, 1995; Chen and Ravichandran 1996, 2000; Sarva and Nemat-Nasser 2001), rock (Perkins and Green 1970; Xia et al. 2008; Dai et al. 2010), ductile materials like steel (Davis and Hunter 1963; Singh et al. 2008 (impact testing); Zhang et al. 2011) and particulate materials like soil (Veyera and Ross 1995). Perkins and Green (1970) performed uniaxial compression tests at strain rates from 10^{-4} to 10^4/s on three geological materials. They also conducted uniaxial compressive strength tests on porphyritic tonalite at strain rates up to 10^3/s and at varying temperatures. They observed that rocks exhibit increased stiffness and higher stress with increasing strain rate and decreasing temperature. Christensen et al. (1972) performed SHPB tests on nugget sandstone at strain rates from 10^2 to 10^3/s at confining pressure of 206.84 MPa. All rocks showed an increase in strength with increasing loading rate. The dynamic stress–strain curves of rocks exhibited similar trends as observed in quasi-static testing of the same materials. Dynamic strength and fracture properties of Dresser basalt were studied by Lindholm et al. (1974) by performing uniaxial compression and extension tests with radial confining pressure varying from 0 to 689.47 MPa for strain rates varying from 10^{-4} to 10^3/s and temperatures varying from 80 to 1400 K. A strong dependence of the ultimate or fracture strength on both temperature and rate of

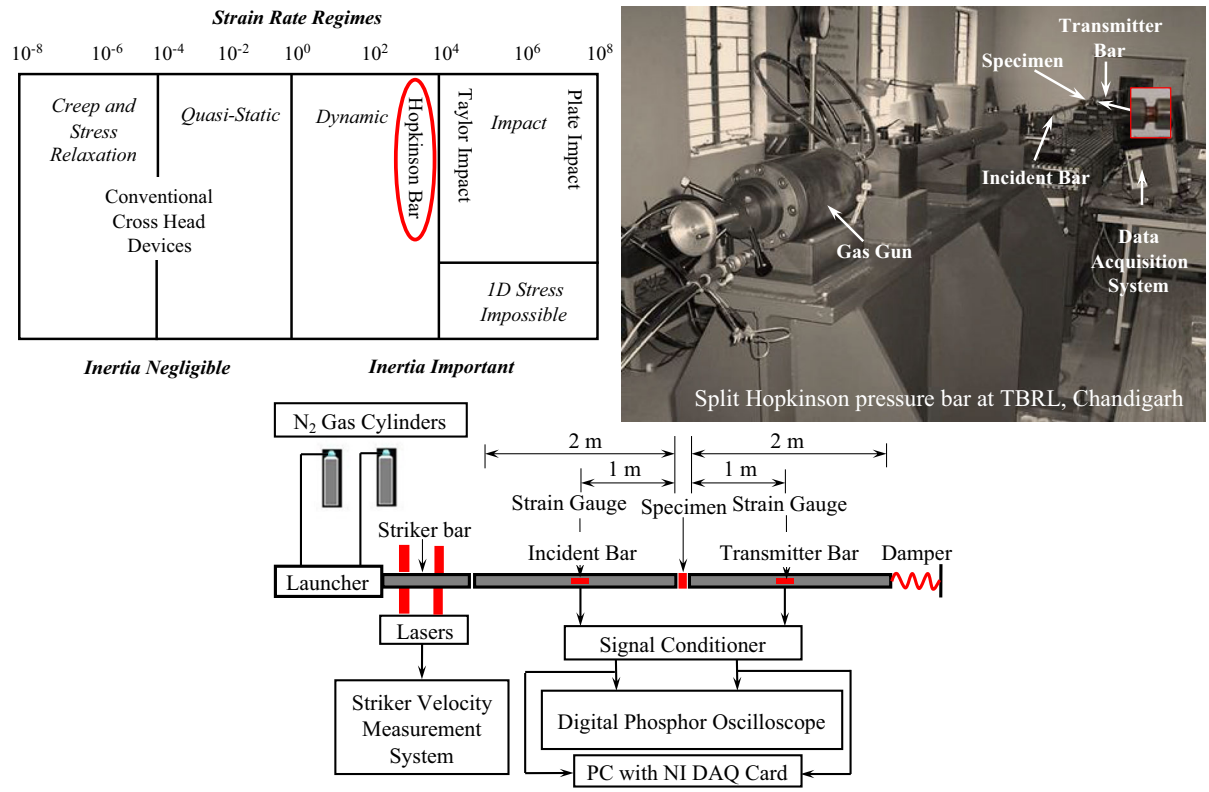

Fig. 1 Schematic diagram for different strain rate regime and the techniques adopted for various tests

deformation was observed from the test results. Blanton (1981) performed dynamic triaxial compression tests at strain rates varying from 10^{-2} to 10/s for charcoal granodiorite up to a confining pressure of 0.45 GPa and for Berea sandstone and Indiana limestone up to a confining pressure of 0.25 GPa. The results showed that the differential stress at failure is relatively constant up to a strain rate of 1/s; however, it increases drastically when the strain rate becomes greater than 1/s. High strain rate response of viscoelastic and quasi-brittle materials such as coal and mortar was studied by Klepaczko (1990). It was observed that brittle material like rock shows a relatively high rate of sensitivity from 1000/s strain rate. However, technical difficulties were faced to get the strain rate above 1000/s strain rate. Olsson (1991) performed SHPB tests on hard volcanic tuff with strain rates varying from 10^{-6} to 10^{3}/s. It was observed from the results that the strength of rock is a weak function of strain rate varying from 10^{-6} to 76/s; however, for strain rate above 76/s, the strength increases significantly with strain rate.

The tests discussed above suffered from major limitations of inertial effect and frictional effect which resulted in stress non-uniformity. To achieve stress uniformity and to avoid multiple loading of the sample, pulse shaping technique was adopted for the first time by Nemant-Nasser et al. (1991) which enabled single pulse loading (1D wave propagation). Pulse shaping technique for rocks, e.g. limestone was adopted by Frew et al. (2001). Dynamic stress–strain response of Bukit Timah granite loaded at a medium strain rate of 20–60/s in split Hopkinson pressure bar apparatus has been reported by Li and Meng (2003). It was observed from the results that the dynamic fracture strength of the granite loaded at medium strain rate is directly proportional to the cube root of strain rate whereas the elastic modulus remains unchanged with increasing strain rate. At higher strain rate, the rocks show a higher amount of energy absorption and hence, the size of the fragments at the end of the test becomes smaller. Fukui et al. (2004) performed strain rate dependent shear strength test of Sanjome andesite. It was observed from their tests that the shear strength of rock is significantly dependent on loading rate. Moreover, if loading rate is increased by an order of magnitude, the cohesion of rock increases by 6.1% and this rate of increase of cohesion remains approximately same for uniaxial compressive strength, uniaxial tensile strength, indirect tensile strength and fracture toughness.

The measure of strength increase of the rocks is defined by dynamic increase factor (*DIF*) which signifies the increase in strength of the rock due to dynamic loading with respect to static loading given by

$$DIF = \frac{Peak\ stress\ due\ to\ rate\ dependent\ loading\ (\sigma_{dc})}{Peak\ stress\ due\ to\ static\ loading\ (\sigma_{c})}. \quad (1)$$

Several researchers in the past have proposed different equations for *DIF* through experimental and numerical studies which are summarized in Table 1. It may be observed from Table 1 that the *DIF* equations of rock are logarithmic functions of strain rate. It is seen that the *DIF* lines proposed by various researchers are very close to each other above 1/s strain rate. However, below 1/s strain rate, different rocks exhibit different rates of strength increase with increasing strain rate. It may be summarized from the literature that the dynamic compressive strength tests on rocks using SHPB device have been carried out on different rock types, e.g. granite, Barre granite, basalt, volcanic tuff, Kawazu tuff, red sandstone, Indiana limestone, porphyritic tonalite, oil shale, granodiorite, coal, kidney stone, Tennessee marble and Akyoshi marble up to 2000/s strain rate (Lu et al. 2010). However, SHPB test data above 2000/s on Indian rocks is currently unavailable in the literature. Hence, the test data produced will be useful in developing rate-dependent constitutive models for rock. The equation thus proposed for dynamic increase factor with respect to strain rate can also be used in blast resistant design for underground structures when the structure is to be built in that specific kind of rock.

The objectives of the present work are (1) to investigate the dynamic and static uniaxial compressive strengths of eight Indian sedimentary and metamorphic rocks used in civil infrastructure through SHPB and static uniaxial testing, respectively, (2) to study the peak stress and strain at peak stress of the rocks under increasing strain rate and (3) to propose an equation for dynamic increase factor (*DIF*) for rocks tested in the present work. The behavior of eight rocks from different regions of India, e.g. Kota sandstone, Dholpur sandstone, Kota limestone, Himalayan limestone, dolomite, quartzite, quartzitic gneiss, and

Table 1 *DIF* proposed by various researchers in the literature

Zhou and Hao (2008)	$DIF = 0.0225\,(\log \dot{\varepsilon}) + 1.12$ for $\dot{\varepsilon} \le 10/\mathrm{s}$
	$DIF = 0.2713\,(\log \dot{\varepsilon})^2 - 0.3563\,(\log \dot{\varepsilon}) + 1.2275$ for $10/\mathrm{s} \le \dot{\varepsilon} \le 2000/\mathrm{s}$
Hao and Hao (2012) (data for various rocks collected from the literature)	$DIF = 0.0523\,(\log \dot{\varepsilon}) + 1.3138$ for $10^{-6}/\mathrm{s} \le \dot{\varepsilon} \le 200/\mathrm{s}$
	$DIF = 2.647551\,(\log \dot{\varepsilon})^2 - 11.766372\,(\log \dot{\varepsilon}) + 14.471157$ for $200/\mathrm{s} \le \dot{\varepsilon} \le 1000/\mathrm{s}$
Hao and Hao (2012), for granite	$DIF_{\mathrm{G}} = 0.018668\,(\log \dot{\varepsilon}) + 1.291887$ for $1/\mathrm{s} \le \dot{\varepsilon} \le 220/\mathrm{s}$
	$DIF_{\mathrm{G}} = 1.8547(\log \dot{\varepsilon})^2 - 7.9014(\log \dot{\varepsilon}) + 9.6647$ for $220/\mathrm{s} \le \dot{\varepsilon} \le 1000/\mathrm{s}$
Hao and Hao (2012), for tuff	$DIF_{\mathrm{T}} = 0.0237\,(\log \dot{\varepsilon}) + 1.2791$ for $1/\mathrm{s} \le \dot{\varepsilon} \le 220/\mathrm{s}$
	$DIF_{\mathrm{T}} = 1.297645\,(\log \dot{\varepsilon})^2 - 5.89126\,(\log \dot{\varepsilon}) + 8.014333$ for $220/\mathrm{s} \le \dot{\varepsilon} \le 1000/\mathrm{s}$
Hao and Hao (2012), for limestone	$DIF_{\mathrm{L}} = 0.0262\,(\log \dot{\varepsilon}) + 1.2827$ for $1/\mathrm{s} \le \dot{\varepsilon} \le 220/\mathrm{s}$
	$DIF_{\mathrm{L}} = 1.898704\,(\log \dot{\varepsilon})^2 - 8.46954\,(\log \dot{\varepsilon}) + 10.76523$ for $220/\mathrm{s} \le \dot{\varepsilon} \le 1000/\mathrm{s}$
Alam et al. (2015), for Kota sandstone	$DIF = 1.16\,(\log \dot{\varepsilon}) + 1.55$ for $10^{-4}/\mathrm{s} \le \dot{\varepsilon} \le 1/\mathrm{s}$
Chakraborty et al. (2016), for quartzite	$DIF = 0.012(\dot{\varepsilon}) + 2.48$ for $77/\mathrm{s} \le \dot{\varepsilon} \le 316/\mathrm{s}$
Chakraborty et al. (2016), for limestone	$DIF = 0.013(\dot{\varepsilon}) + 4.19$ for $60/\mathrm{s} \le \dot{\varepsilon} \le 263/\mathrm{s}$

phyllite have been investigated through SHPB tests at high strain rates up to 2247/s. It may be noted that in the literature, SHPB tests on sandstone has been reported up to a strain rate of 3/s and that for limestone up to a strain rate of 3237/s (Lu et al. 2010). Thus, high strain rate characterization of sandstone up to a strain rate of 2247/s has been carried out in the present work for the first time in the literature.

2 Test Plan for Static and Dynamic Tests

In the present work, the investigations are carried out in four different stages, i.e. determination of (1) physical properties, (2) petrological studies, (3) static stress–strain response and (4) dynamic stress–strain response of the rocks. The detailed test plan for all the four different stages is presented in Fig. 2. The rocks are collected from various important project sites of national importance from different regions of India e.g. sandstones are collected from Kota and Dholpur city from Rajasthan; limestones are collected from Kota, Rajasthan and Kol Dam, Himachal Pradesh (Kol Dam is situated in the foothills of the Himalayas in Shivalik range); dolomite and quartzite are collected from Kol Dam, Rajasthan; quartzitic gneiss is collected from Almora barrage, Uttarakhand and, phyllite is collected from T48 tunnel, Ramban, Jammu. The samples are prepared by following ISRM and ASTM standards for the different tests to be conducted and are shown in Fig. 3. Among the physical properties of the rocks, the dry density and specific gravity of the rocks have been determined. Petrological studies of the rocks have been carried out through X-ray diffraction (XRD) test and scanning electron microscope (SEM) test. The static stress–strain behavior of the rocks under compressive and tensile loading has been determined through unconfined compressive strength (UCS) test, and point load test, respectively. Table 2 presents the regions from where the rocks were collected, physical properties of the rocks, the static uniaxial compressive strength of rocks, static elastic modulus and the point load index. The dynamic stress–strain response of the rocks is investigated through compressive SHPB test by following ISRM standards (Zhou et al. 2011) at four to six different strain rates for each rock type as shown in Table 3. The rock samples of 18 mm diameter and slenderness ratio of 0.5 are prepared and 10 samples from each rock type are tested among which only 4–6 samples from each rock type has reached stress equilibrium and trapezoidal stress pulse is observed. The trapezoidal stress pulse is recorded on the oscilloscope upon loading the samples dynamically by using SHPB device. The SHPB device used in the present work is of 20 mm diameter and this generates a very high strain rate due to the smaller diameter of the bars. The minimum propulsion limit of the gas gun to the striker bar is 0.05 MPa. Due to the

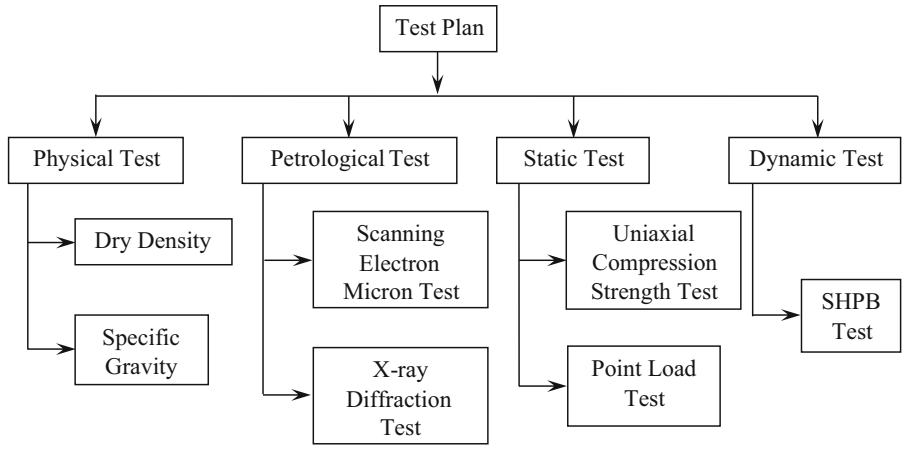

Fig. 2 Test plan for the five sedimentary and three metamorphic rocks

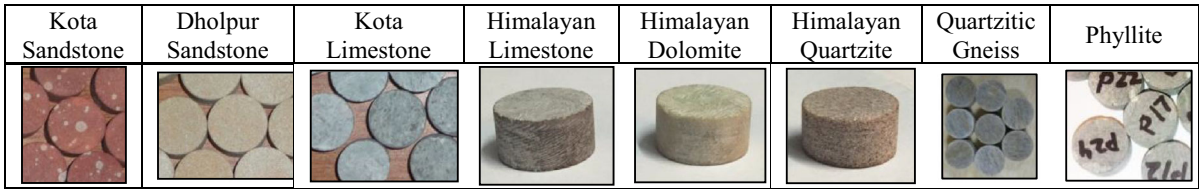

Fig. 3 Photographs of finished samples of the rocks collected

Table 2 Physical and static properties

Rocks	Region	Dry density, ρ_d (kg/m^3)	Specific gravity, G	Uniaxial compressive strength[a], σ_c (MPa)	Elastic modulus, E_t (GPa)	Point Load index, I_s
Sandstone	Kota, Rajasthan	2588.22	2.63	39.64	1.53	1.91
	Dholpur, Rajasthan	2631.22	2.64	39.30	1.48	1.92
Limestone	Kota, Rajasthan	2668.48	2.72	45.90	1.72	2.21
	Kol Dam, Himachal Pradesh	2630.60	2.71	51.21	2.62	2.43
Dolomite	Kol Dam, Himachal Pradesh	2731.82	2.70	38.59	3.75	1.88
Quartzite	Kol Dam, Himachal Pradesh	2585.80	2.80	108.20	11.60	4.88
Quartzitic Gneiss	Almora, Uttarakhand	2615.00	2.66	76.71	10.21	3.65
Phyllite	Ramban, Jammu	2758.00	2.80	63.25	14.58	2.87

[a] At a strain rate of 0.001 per second

specimen size and heterogeneity, it gets crushed at this strain rate range of above 1000/s. Hence, it becomes very difficult to achieve force equilibrium and obtain a correct stress–strain response. Therefore, the force equilibrium results are obtained for 4–6 samples from a total of 10 samples prepared. The static tests have been performed in the Rock Engineering Laboratory of Indian Institute of Technology (IIT) Delhi. The

Table 3 Test plan for SHPB test

Rocks	Region	No. of samples tested	Length of the striker bar (mm)	Strain rate achieved (/s)
Sandstone	Kota, Rajasthan	10	300	1550
				1663
				2100
				2247
	Dholpur, Rajasthan	10	300	1570
				1600
				1800
				1930
Limestone	Kota, Rajasthan	10	300	1219
				1676
				1781
				2057
	Kol Dam, Himachal Pradesh	10	300	695
				1304
				1422
				1463
Dolomite	Kol Dam, Himachal Pradesh	10	300	478
				1021
				1139
				1222
Quartzite	Kol Dam, Himachal Pradesh	10	300	553
				723
				869
				921
Quartzitic Gneiss	Almora, Uttarakhand	10	300	323
				370
				550
				710
				877
				985
Phyllite	Ramban, Jammu	10	300	534
				540
				1217
				1629

SHPB tests have been carried out in the Terminal Ballistics Research Laboratory (TBRL), Chandigarh, India. The dynamic peak stress of the rocks has been compared with that obtained from the static tests for calculating the *DIF*. Correlation equations for *DIF* with strain rate has been proposed for sandstone, limestone, dolomite, quartzite, quartzitic gneiss and phyllite.

3 Test Setup for Compressive Uniaxial Test and Point Load Test

3.1 Automatic Compressive Uniaxial Test Machine

The automatic compressive uniaxial test machine used in the present study is from Hydraulic and Engineering

(a) Automatic Uniaxial Compression Machine **(b)** Point Load Apparatus

Fig. 4 Machines used for static characterization

Instruments (HEICO) company and is shown in Fig. 4a. It consists of a loading frame, a pumping unit, and a data acquisition system. The equipment is checked according to procedures given in ASTM standards of practices E4 (ASTM E4-16 2016). The capacity of the automatic compression machine is 3000 kN with a maximum daylight clearance of 500 mm and ram travel of 50 mm. The loading frame consists of two loading platens. The lower platen holds the hydraulic ram to load the specimen and the upper platen has the spherical seating to take care of any irregularity of the specimen surface or slight misplacement of the specimen from the central position. The pumping unit has an arrangement for automatic compression system which is achieved by the combination of advanced hydraulic and electronic system. The control signal from the electronic system is passed on to the high-speed proportional valve, which in turn controls the flow of oil into the compression rate constant irrespective of any change that occurs in the specimen during the process of testing. The compression rate is set on strain or stress basis. The tests are conducted with a maximum stroke rate of 10/s. There are many experimental techniques available for characterizing a material in different strain rate regime as shown by Field et al. (2004) in Fig. 1. The strain rate considered for static characterization of material is from 10^{-4} to 1/s. The tests conducted in the present work is at a rate of 0.001/s strain rate. The load is automatically released after the peak value is achieved. The data acquisition system captures the stress versus strain response which is further analyzed to get peak stress and elastic modulus of the rock specimen tested.

3.2 Point Load Apparatus

The point load testing apparatus consists of a loading frame, two truncated conical platens and a measuring system to measure the applied load, *P*. The point load apparatus used in the present study is from Hydraulic and Engineering Instruments (HEICO) company and has a capacity of 100 kN. It is shown in Fig. 4b with the point load tester. The unit comprises of a base frame on which the frame assembly with the integral jack and two load gauges with isolating valves are fixed. The ram of the jack carries the lower cone while the upper cross head has the other loading cone. The cones are made as per IS 8764. Spacer blocks are provided to test samples ranging from EX size to 100 mm size. Maximum clearance between the two cones is approx 125 mm. Lower range gauge of 25 kN is provided for better sensitivity and 100 kN gauge reaches up to the maximum capacity. In the present

work, the specimen of 1:1 slenderness ratio is prepared to determine the point load index (D5731-08 2008). The specimen is placed axially between the two truncated conical platens of the point load tester. The dial gage on the measuring system indicates the failure load of the specimen. The point load index is then calculated by using the failure load and the diameter of the specimen.

4 Test Setup for Split Hopkinson Pressure Bar

The split Hopkinson pressure bar apparatus in TBRL Chandigarh consists of three bars designated as striker bar, incident bar, and transmitter bar. Figure 1 shows the photograph of the SHPB setup in TBRL and presents a schematic diagram of the compressive SHPB setup. The cylindrical rock sample is sandwiched between the incident and the transmitter bars when a longitudinal compressive wave generated by the impact of striker bar propagates through the incident bar. This compressive wave passes through the rock sample which creates a high rate of loading on the rock sample. At the incident bar—rock sample interface, a part of the incident wave is reflected and a part is transmitted through the sample to the transmitter bar. The bars are made up of high strength maraging steel having a yield strength of $\sim$1750 MPa. The length of the incident bar and the transmitter bar are 2000 mm each while the diameter of striker bar, incident bar, and transmitter bar is 20 mm each. Herein, 10 samples of each rock with 18 mm diameter and slenderness ratio, e.g. length to diameter (L/D) = 0.5:1 have been prepared for the dynamic experiments to perform the test at varying strain rates. The slenderness ratio of 0.5 is taken to reduce the axial inertial effect and attain force equilibrium (Gray 2000; Frew et al. 2001; Xia and Yao 2015). The compressive SHPB tests are based on two fundamental assumptions—(a) one-dimensional (1D) elastic wave propagation in the bars and (b) homogeneous deformation of the sample (Zhou and Zhao 2011). The 1D wave propagation has been ensured herein by using long incident and transmission bars. The elastic deformation of the bars is taken care by limiting the impact velocity of the striker. This striker bar upon impacting the end of the incident bar generates a strain pulse that does not affect the yield strength of the incident and transmission bars. Proper alignment of the bars is required for satisfying the fundamental assumption of uniform deformation and one-dimensional wave propagation within the bars as well as uniaxial compression within the sample during loading. For this, bearing and alignment fixtures have been used to allow the bars and the striking projectile to move freely while retaining precise axial alignment. A 300 mm long projectile has been used as a striker bar and is propelled towards the incident bar using compressed nitrogen gas launcher. Two photosensors located at a distance of 100 mm apart from the nozzle end of the gun barrel are used to measure the impact velocity of the striker bar. The impact of the striker bar on the incident bar causes a longitudinal elastic compressive stress wave which propagates through the incident bar. The strain pulse generated within the incident bar is designated as incident strain pulse $\varepsilon_i(t)$. Upon reaching the incident bar—sample interface, a part of the pulse, designated as reflected strain pulse $\varepsilon_r(t)$ is reflected back in the incident bar and the remaining of the compressive pulse passes through the sample. Upon reaching the interface of the sample and the transmitter bar, the pulse propagates through transmitter bar and it is then termed as transmitted wave, $\varepsilon_t(t)$. The time histories of strain $\varepsilon(t)$, strain rate $\dot{\varepsilon}(t)$ and stress $\sigma(t)$ within the sample in the dynamic compression test are given by

$$\varepsilon(t) = \frac{C}{L}\int_0^t (\varepsilon_i - \varepsilon_r - \varepsilon_t)dt \tag{2}$$

$$\dot{\varepsilon}(t) = \frac{C}{L}(\varepsilon_i - \varepsilon_r - \varepsilon_t) \tag{3}$$

$$\sigma(t) = \frac{A}{2A_0}E(\varepsilon_i + \varepsilon_r + \varepsilon_t) \tag{4}$$

where L is the length of the sample, C is the one-dimensional longitudinal stress wave velocity of the bar, A is the cross-sectional area of the bar, E is Young's modulus of the bar and A_0 is the initial area of the sample. Assuming that the stress equilibrium and the uniform deformation of the sample prevail during dynamic loading, i.e. $\varepsilon_i + \varepsilon_r = \varepsilon_t$, the strain, strain rate, and stress are given by

$$\varepsilon(t) = -\frac{C}{L}\int_0^t \varepsilon_r dt \tag{5}$$

$$\dot{\varepsilon}(t) = -\frac{C}{L}\varepsilon_r \tag{6}$$

$$\sigma(t) = \frac{A}{A_0}E\varepsilon_t \tag{7}$$

4.1 Data Acquisition System

The time of passage and the amplitude of the three pulses mentioned above are recorded by precision strain gauges of type EA-06-125TM-120 with 120 Ω resistance, 90° tee rosette mounted at the mid-point positions along the length of the two bars. The strain gauges are mounted on the bars using M-Bond 200 strain gauge adhesive glue from Vishay Micro-Measurements, USA. Strain–time signals in the incident and transmitter bars are recorded by 2210A signal conditioning amplifier system (Measurements group Inc., USA) and National Instruments Data Acquisition 6111-E card based data acquisition system with LABVIEW® 6.1 software. The strain gauges are used in the full-bridge configuration for the maximum output signal.

4.2 Pulse Shaper

It was observed during the tests that the rectangular shaped incident pulse generated in the incident bar may form a steep rise in stress level and thus can impose a non-uniform strain rate during elastic deformation of the sample caused by the difference in the slopes of incident loading rate and stress–strain response of the test sample. Therefore, to modify the incident pulse shape for obtaining the elastic response of the test sample, a ramp pulse is produced by placing a 1 mm thick copper disk of 12 mm diameter on the impact end of the incident bar. This also helps in filtering out the undesired oscillations in the incident signal.

5 Results and Discussion

5.1 Physical Properties

To determine the physical properties of the rocks, the dry density and specific gravity have been estimated for three samples of each rock type. The average dry density and specific gravity of Kota sandstone, Dholpur sandstone, Kota limestone, Himalayan limestone, quartzite, quartzitic gneiss, and phyllite are presented in Table 2. The density and specific gravity values of all the eight rocks are compared with the available data from the literature and the data are found to be in close agreement (Kumar 2007; Anuradha et al. 2016).

5.2 Petrological Data

Petrological studies of the eight rocks are carried out to identify the origin, composition and distribution of rocks using the XRD and SEM techniques. The petrological data define the mineral content of the rock which in turn describe the geological properties of the rock. Thus, from the mineral content, it can be predicted whether a rock would behave as brittle or ductile material upon loading. The basic physics that explains the increase in strength of rock when tested using SHPB device is explained as follows. It has been observed from the literature that a material when tested under dynamic loads, gives the following combination of response—(a) peak stress is strain rate sensitive whereas elastic modulus is not, (b) elastic modulus is strain rate sensitive whereas peak stress is not, and (c) peak stress and elastic modulus both are strain rate sensitive. The failure mechanism of rock is a complex issue due to the anisotropic nature of the rock (Zhu et al. 2012). For an anisotropic medium, the complications occur due to the directionality of the bulk moduli resulting in contribution to damage. Rocks can be classified as brittle or ductile depending on its mineralogy. The response of the rock subjected to impact loading depends on its mineralogy. The igneous rock being the intrusive and parent rock contains clay and may exhibit higher dynamic increase factor than sedimentary or metamorphic rock (Tyrell 1978). Due to the presence of clay content, localized plastic deformation of the rock is observed when tested dynamically by using SHPB device. The presence of clay as a binding material in rock increases the flow stress of the rock. This results in an increase in the dynamic increase factor. When the rocks are assessed in terms of ductility in ascending order, the igneous rock is more ductile than the sedimentary rock in terms of binding material as clay content and sedimentary rock is more ductile than metamorphic

rock. Metamorphic rocks are made up of interlocking of grains. The metamorphic rock can take strain up to the lock up strain of the grains while the igneous and sedimentary rocks can take more strain due to the clay content in it. The ductility decreases from igneous to metamorphic rocks. Due to higher clay content in igneous rock, its dynamic increase factor (e.g. ratio of dynamic peak strength to static strength) is much higher than that of the metamorphic rocks as observed in the literature (Lu et al. 2010). The failure models for brittle materials require several important features, including a definition of damage, a description of degraded moduli, micro crack distribution, micro crack growth laws and micro crack coalescence. Whereas for ductile materials, the fundamental failure mechanism is related to dynamic fracture and the failure process initiated by nucleation of voids around inclusions, their subsequent growth, and coalescence. Hence, in order to know the mineralogy of the rock tested, scanning electron microscope and X-ray diffraction tests are needed relating to dynamic increase factor. Figure 5 shows the scanning electron microscope (SEM) images and X-ray diffraction graphs for Kota sandstone, Dholpur sandstone, Kota limestone, Himalayan limestone, dolomite, Himalayan quartzite, quartzitic gneiss and phyllite. The XRD graphs of all the eight rocks are compared with the available data from the literature and it is found to be in close agreement (Kumar 2007). It is observed that the Kota sandstone which is red in color, contains almost 97% of quartz and magnetite clay (1–2%) with clay minerals (1%), illite and iron oxide. Dholpur sandstone which is pink in color, contains primarily quartz (90%) and muscovite (1%) with iron oxide and clay minerals. Kota limestone which is gray in color contains primarily calcite (60%), iron oxide and clay minerals (10–11%). It is seen that Himalayan limestone which is transversely banded with dark and light pink color, shows the presence of minerals such as carbonate (90%), clay minerals like illite and kaolinite (7%), quartz (2%) and chlorite (1%). Dolomite is very light yellow in color and contains mainly carbonate in higher quantity (92%), some clay minerals like sepiolite, kaolinite and illite in smaller quantities (7%) and quartz (1%). Metamorphic rock is identified by its amorphous structure from SEM images. Quartzite is light red in color, contains minerals like quartz in higher quantity (89%) and some other minerals such as chlorite, feldspar, mica and kaolin in smaller quantities (11%). It is investigated by the physical observation that quartzitic gneiss is very opaque and white in color and contains a very high percentage of quartz (90%), carbonate and kaolinite minerals. Phyllite which is dark green in color, contains a feldspar in higher quantity (88%), attapulgite, chlorite, carbonate and some clay minerals like kaolinite and illite (5%). In the present study, the diameter of the specimen is very small i.e. 18 mm. The specimens are crushed to powder form at the strain rate tested. Hence, post-SEM is not possible for the crushed samples. Now, there are three types of response that is yielded when a specimen is tested under high strain rate loading—(1) the peak stress is strain rate sensitive whereas the elastic modulus is not, (2) the elastic modulus is strain rate sensitive whereas the peak stress is not, and (3) the peak stress and elastic modulus both are strain rate sensitive. In the present study, the Kota sandstone, Kota limestone, Himalayan quartzite and Quartzitic gneiss shows peak stress and elastic modulus sensitivity to strain rate. Whereas, Dholpur sandstone, Himalayan limestone, Himalayan dolomite and phyllite show only peak stress sensitivity to strain rate. This is explained by the presence of clay in Dholpur sandstone, Himalayan limestone, Himalayan dolomite and phyllite. The clay absorbs the higher rate of loading and keeps the elastic modulus constant increasing the peak stress.

5.3 Static Mechanical Properties

Static uniaxial compression tests of the eight rocks have been performed at a strain rate of 0.001/s. The samples are prepared with a slenderness ratio of 2:1 as defined in ASTM standards (ASTM D4543-08 2008). For each rock type, three rock samples are tested for better reproducibility of the results. The static tensile strength of the rocks has been determined through point load test. Table 2 presents the static uniaxial compressive strength of rock, static modulus of elasticity and the point load index. ASTM D7012-14 (2014) is followed herein to calculate the elastic modulus of the rock at 50% of the peak stress. It is seen that the uniaxial compressive strength of the rocks are found to be 39.64 MPa for Kota sandstone, 39.30 MPa for Dholpur sandstone, 45.90 MPa for Kota limestone, 51.21 MPa for Himalayan limestone, 38.59 MPa for dolomite, 108.20 MPa for quartzite, 76.71 MPa for quartzitic gneiss and 63.25 MPa for phyllite. The

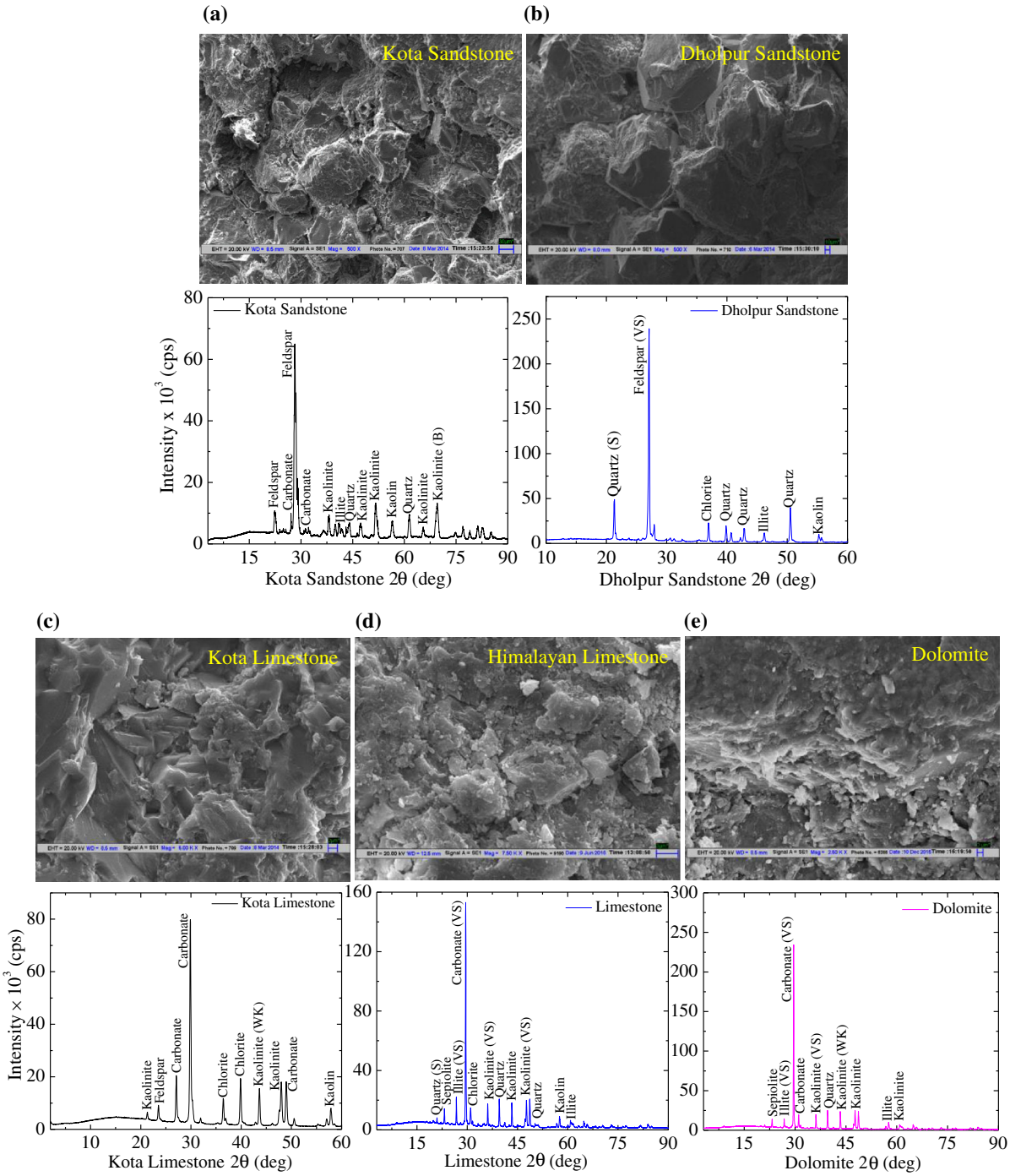

Fig. 5 Scanning electron microscope (SEM) image and X-ray diffraction (XRD) graph of **a** Kota sandstone, **b** Dholpur sandstone, **c** Kota limestone, **d** Himalayan limestone, **e** dolomite, **f** quartzite, **g** quartzite gneiss, and **h** phyllite

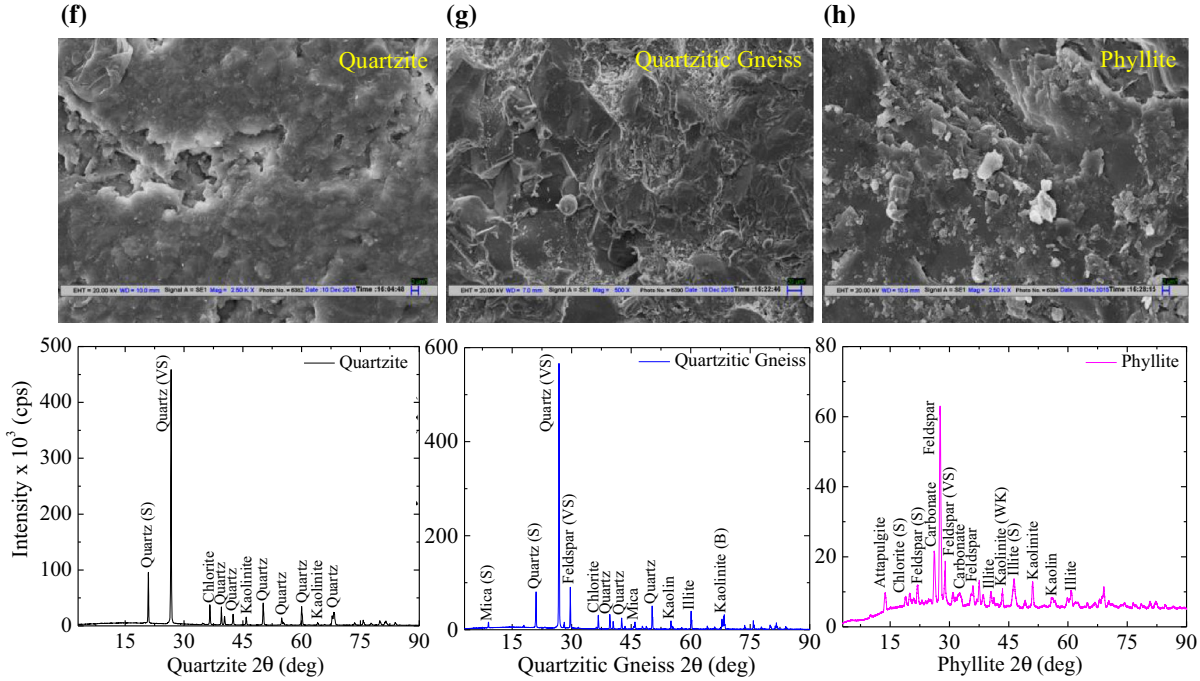

Fig. 5 continued

elastic modulus are determined to be 1.53 GPa for Kota sandstone, 1.48 GPa for Dholpur sandstone, 1.72 GPa for Kota limestone, 2.62 GPa for Himalayan limestone, 3.75 GPa for dolomite, 11.60 GPa for quartzite, 10.21 GPa for quartzitic gneiss and 14.58 GPa for phyllite. It is observed that the UCS value of sedimentary rocks is less than that of the metamorphic rocks. This is explained by the fact that the metamorphic rocks are formed by the metamorphosis of sedimentary rock minerals. Hence, under the action of extreme heat and temperature, the strength of the metamorphic rock minerals increases to 2.5 times the strength of sedimentary rock minerals. This phenomenon also explains the higher elastic modulus for metamorphic rocks than sedimentary rocks. It is also seen that the rocks such as sandstone and limestone collected from different regions of India exhibit similar UCS and elastic modulus values. The uniaxial compressive strength of the sedimentary rocks and metamorphic rocks are found to be in the universal range of 30–70 and 50–180 MPa, respectively. The ratios of uniaxial compressive stress to point load index for all the eight rocks are well within the range of 20–25 as specified in International Society of Rock Mechanics (ISRM) standard (ISRM 1985; Akram and Bakar 2007). The uniaxial compressive strength and point load index for all the eight rocks are compared with the available data from the literature and it is found to be in close agreement (Kumar 2007; Anuradha et al. 2016).

5.4 Dynamic Mechanical Properties

All the eight types of rocks are tested for dynamic compressive strength at high strain rates from 300 to 2247/s in the SHPB device. The upper limit of strain rate and the slenderness ratio is computed analytically by using the available relations for the length of sample with the limiting strain rate. Taking the failure strain, ε_f to be 1%, the upper limit of strain rate is presented (Ravichandran and Subhash 1994) as

$$\dot{\varepsilon}_1 = \frac{\varepsilon_f c}{\alpha L} \tag{8}$$

where c is the elastic wave speed of the specimen, L is the length of the specimen and α is a non dimensional parameter which depends on the shape of the incident

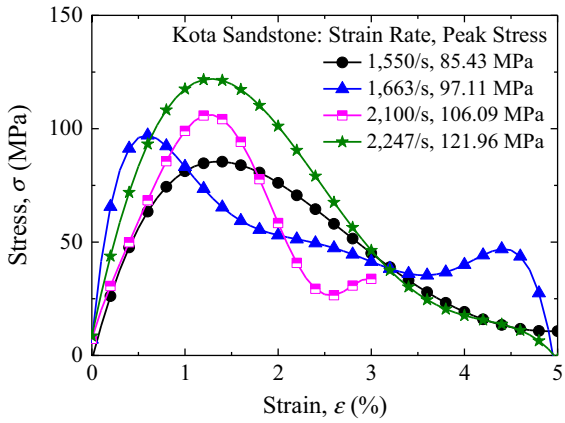

Fig. 6 Stress–strain response of Kota sandstone

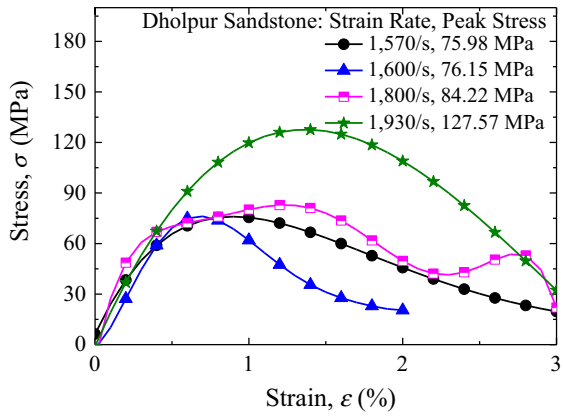

Fig. 7 Stress–strain response of Dholpur sandstone

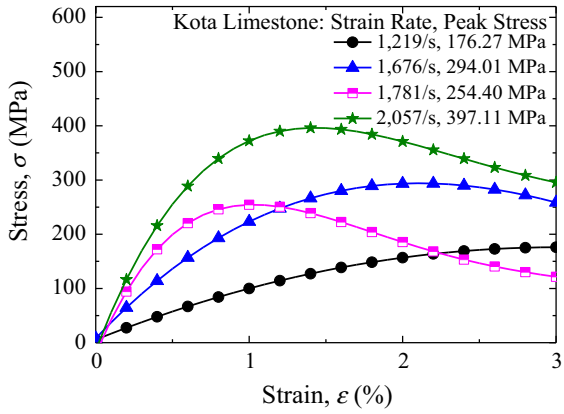

Fig. 8 Stress–strain response of Kota limestone

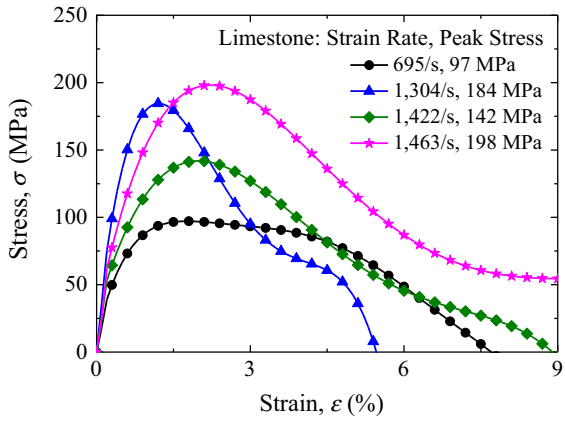

Fig. 9 Stress–strain response of Himalayan limestone

pulse. Above this limiting strain, the true value of stress–strain response is not obtained. Hence, the highest strain rate that can be reached depends on the material parameters. The stress–strain curves have been plotted for each rock type at different strain rates and the peak stresses are noted. Figures 6, 7, 8, 9, 10, 11, 12, and 13 show the stress–strain response for Kota sandstone, Dholpur sandstone, Kota limestone, Himalayan limestone, quartzite, quartzitic gneiss, and phyllite, respectively.

Figure 6 shows the stress–strain response of Kota sandstone for different strain rates from 1550 to 2247/s. The peak stress obtained are 85.43 MPa at 1550/s, 97.11 MPa at 1663/s, 106.09 MPa at 2100/s and 121.96 MPa at 2247/s which signifies that the peak stress increases with increasing strain rate. The peak stress, strain at peak stress and *DIF* results of Kota sandstone are presented in Table 4. The increasing trend of dynamic peak stress with increasing strain rate can be seen more clearly from Table 4. It may be observed that the peak stress increases at a rate of 13–14% till the strain rate of 1800/s, however, it increases abruptly by 25–45% above 1800/s strain rate. The peak stress of the rocks increases rapidly with an increase in the loading rate from quasi-static to dynamic. The dynamic compressive stress 121.96 MPa at 2247/s is nearly thrice as compared to the static compressive stress. Moreover, it may be noted from Table 4 that the strain at peak stress does not exhibit any dependence on strain rate in these dynamic tests. In the present study, the size of the rock specimen is very small e.g. 18 mm and heterogeneous. It is tested at a very higher strain of more than 1000/s exhibiting an increase in peak strength with increase in strain rate. The deviation of elastic modulus for the sample tested at 1663/s strain rate is due to the

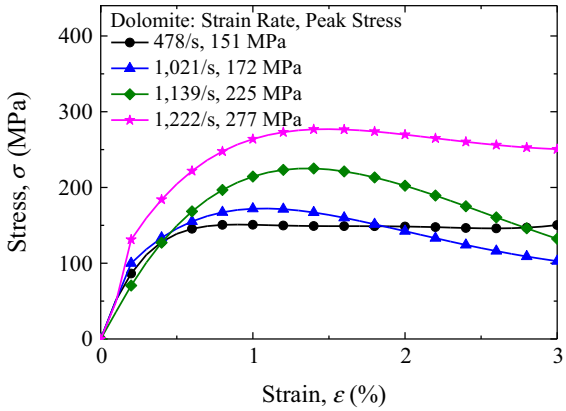

Fig. 10 Stress–strain response of dolomite

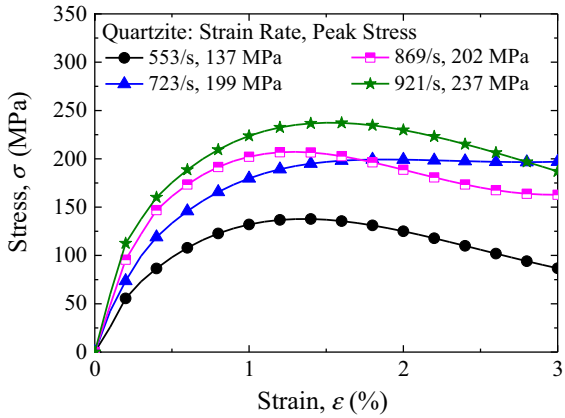

Fig. 11 Stress–strain response of quartzite

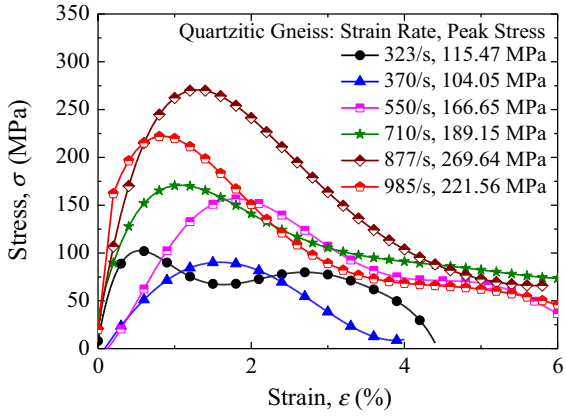

Fig. 12 Stress–strain response of quartzitic gneiss

sampling procedure. The sample may contain a harder mineral like quartz giving higher elastic modulus than other samples.

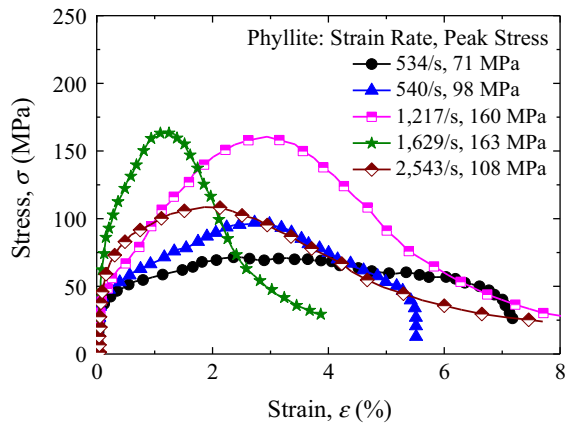

Fig. 13 Stress–strain response of phyllite

Table 4 Dynamic properties: Kota sandstone

Strain rate, $\dot{\varepsilon}$ (/s)	Peak stress, σ_{dc} (MPa)	Strain at peak stress, ε (%)	Dynamic increase factor, *DIF*
1550	85.43	1.20	2.15
1663	97.11	0.63	2.45
2100	106.09	1.00	2.67
2247	121.96	1.06	3.07

Figure 7 shows the stress–strain response of Dholpur sandstone at different strain rates. The peak stress for different strain rates as noted from Fig. 7 are 75.98 MPa at 1570/s, 76.15 MPa at 1600/s, 84.22 MPa at 1800/s and 127.57 MPa at 1930/s. The peak stress, strain at peak stress, elastic modulus and *DIF* results of Dholpur sandstone are presented in Table 5. It can be seen from Table 5 that the peak stress increases slowly at a rate of almost 10% with increasing strain rate up to a strain rate of 1800/s while above 1800/s strain rate, it increases abruptly by 51.47%. The peak stress of the rocks increases rapidly with an increase in the loading rate from quasi-static to dynamic. The dynamic compressive stress 127.57 MPa at 1930/s is more than thrice as compared to the static compressive stress. However, it may be noted from Table 5 that the strain at peak stress does not exhibit any dependence on strain rate in these dynamic tests.

Figure 8 shows the stress–strain response of Kota limestone at different strain rates. The peak stress values obtained at different strain rates as observed

Table 5 Dynamic properties: Dholpur sandstone

Strain rate, $\dot{\varepsilon}$ (/s)	Peak stress, σ_{dc} (MPa)	Strain at peak stress, ε (%)	Dynamic increase factor, *DIF*
1570	75.98	1.07	1.93
1600	76.15	0.77	1.94
1800	84.22	1.30	2.14
1930	127.57	1.27	3.24

Table 6 Dynamic properties: Kota limestone

Strain rate, $\dot{\varepsilon}$ (/s)	Peak stress, σ_{dc} (MPa)	Strain at peak stress, ε (%)	Dynamic increase factor, *DIF*
1219	176.27	3.17	3.84
1676	294.01	1.93	6.41
1781	254.40	1.02	5.54
2057	397.11	1.24	8.65

Table 7 Dynamic properties: Himalayan limestone

Strain rate, $\dot{\varepsilon}$ (/s)	Peak stress, σ_{dc} (MPa)	Strain at peak stress, ε (%)	Dynamic increase factor, *DIF*
695	97	1.41	1.89
1304	184	0.82	3.59
1422	142	2.60	2.77
1463	198	1.76	3.87

Table 8 Dynamic properties: dolomite

Strain rate, $\dot{\varepsilon}$ (/s)	Peak stress, σ_{dc} (MPa)	Strain at peak stress, ε (%)	Dynamic increase factor, *DIF*
478	151	0.9	3.91
1021	172	1	4.45
1139	225	1.4	5.83
1222	277	1.5	7.17

from Fig. 8 are 176.27 MPa at 1219/s, 294.01 MPa at 1676/s, 254.4 MPa at 1781/s and 397.11 MPa at 2057/s. The peak stress, strain at peak stress and *DIF* results of Kota limestone are presented in Table 6. The peak stress increases by 55–70% with each increase in strain rate. The peak stress of the rocks increases rapidly with an increase in the loading rate from quasi-static to dynamic. The dynamic compressive stress 397.11 MPa at 2057/s is more than eight times as compared to the static compressive stress.

Figure 9 presents the stress–strain response of Himalayan limestone at different strain rates. The peak stress values obtained at different strain rates as observed in Fig. 9 are 97.00 MPa at 695/s, 184.00 MPa at 1304/s, 142.00 MPa at 1422/s and 198.00 MPa at 1463/s. The peak stress, strain at peak stress and *DIF* results of Himalayan limestone are presented in Table 7. The peak stress increases by 30–80% with each increase in strain rate which can be seen from Table 7. The dynamic compressive stress 198.00 MPa at 1463/s is nearly four times as compared to the static compressive stress.

Figure 10 shows the stress–strain response of dolomite at different strain rates. The peak stress values obtained at different strain rates as noted from Fig. 10 are 151.00 MPa at 478/s, 172.00 MPa at 1021/s, 225.00 MPa at 1139/s and 277.00 MPa at 1222/s. The peak stress, strain at peak stress and *DIF* results of dolomite are presented in Table 8. The peak stress increases by 15–30% with each increase in strain rate and is seen in Table 8. The dynamic compressive stress 277.00 MPa at 1222/s is slightly more than seven times as compared to the static compressive stress.

Figure 11 shows the stress–strain response of quartzite at different strain rates. The peak stress values obtained at different strain rates as observed from Fig. 11 are 137.00 MPa at 553/s, 199.00 MPa at 723/s, 202.00 MPa at 869/s and 237.00 MPa at 921/s. The peak stress, strain at peak stress and *DIF* results of quartzite are presented in Table 9. The peak stress increases by 45% with an increase in strain rate from 553 to 723/s strain rate whereas it increases at a very low rate of 1.5% with an increase from 723 to 869/s. The peak stress increases by 17% when the strain rate increases from 869 to 921/s. This variation of peak stress with strain rate can be seen Table 9. The dynamic compressive stress 237.00 MPa at 921/s is slightly more than two times as compared to the static compressive stress.

Figure 12 presents the stress–strain response of quartzitic gneiss at different strain rates. The peak stress values obtained at different strain rates as noted from Fig. 12 are 115.00 MPa at 323/s, 104.00 MPa at 370/s, 167.00 MPa at 550/s, 189.00 MPa at 710/s,

Table 9 Dynamic properties: quartzite

Strain rate, $\dot{\varepsilon}$ (/s)	Peak stress, σ_{dc} (MPa)	Strain at peak stress, ε (%)	Dynamic increase factor, *DIF*
553	137	1.06	1.26
723	199	3.45	1.83
869	202	4.50	1.86
921	237	1.37	2.19

Table 10 Dynamic properties: quartzitic gneiss

Strain rate, $\dot{\varepsilon}$ (/s)	Peak stress, σ_{dc} (MPa)	Strain at peak stress, ε (%)	Dynamic increase factor, *DIF*
323	115	0.70	1.49
370	104	1.58	1.35
550	167	1.48	2.17
710	189	0.61	2.46
877	270	2.12	3.51
985	222	0.20	2.89

270.00 MPa at 877/s and 222.00 MPa at 985/s. The peak stress, strain at peak stress and *DIF* results of quartzitic gneiss are presented in Table 10. The peak stress increases by 45–60% with each increase in strain rate and can be seen from Table 10. The dynamic compressive stress 270.00 MPa at 877/s is more than three times as compared to the static compressive stress.

Figure 13 shows the stress–strain response of phyllite at different strain rates. The peak stress values obtained at different strain rates as noted from Fig. 13 are 71.00 MPa at 534/s, 98.00 MPa at 540/s, 160.00 MPa at 1217/s and 163.00 MPa at 1629/s. The peak stress, strain at peak stress and *DIF* results of phyllite are presented in Table 11. The peak stress increases by 38–63% with each increase in strain rate as observed in Table 11. The dynamic compressive stress 163.00 MPa at 1629/s is more than two times as compared to the static compressive stress.

Dynamic strength increase factors have been determined for all eight rocks by comparing the dynamic peak stress with the static peak stress. From Tables 4, 5, 6, 7, 8, 9, 10, and 11, it is seen that the dynamic peak stress of Kota and Dholpur sandstone varies from 1.8 to 2.2 times the static peak stress for a strain rate range of 1500–1800/s whereas the dynamic peak stress increases to around 3–3.5 times of the static peak stress above a strain rate of 1800/s. From Tables 6 and 7, it is observed that the dynamic peak stress of Kota and Himalayan limestone is around 4–6.5 times the static peak stress for a strain rate range of 1200–1750/s, whereas it suddenly increases approximately to 10 times of the static peak stress above a strain rate of 1800/s.

Table 11 Dynamic properties: phyllite

Strain rate, $\dot{\varepsilon}$ (/s)	Peak stress, σ_{dc} (MPa)	Strain at peak stress, ε (%)	Dynamic increase factor, *DIF*
534	71	2.50	1.12
540	98	2.72	1.54
1217	160	2.93	2.52
1629	163	1.64	2.57

A correlation equation has been developed for the calculated dynamic increase factors with strain rate by setting a best-fitted curve through the obtained results satisfying the 95% confidence interval and is shown in Fig. 14. The correlation for sandstone with a coefficient of determination (R^2) = 0.66 is given by

$$DIF = 2.9\ln(\dot{\varepsilon}) - 19.5 \quad \text{for} \quad 1550/\text{s} \le \dot{\varepsilon} \le 2247/\text{s} \tag{9}$$

The correlation for limestone with a coefficient of determination (R^2) = 0.77 is given by

$$DIF = 9.81\ln(\dot{\varepsilon}) - 67.04 \quad \text{for} \quad 1219/\text{s} \le \dot{\varepsilon} \le 2057/\text{s} \tag{10}$$

The correlation for dolomite with a coefficient of determination (R^2) = 0.98 is given by

$$DIF = 14.91\ln(\dot{\varepsilon}) - 98.98 \quad \text{for} \quad 1021/\text{s} \le \dot{\varepsilon} \le 1222/\text{s} \tag{11}$$

The correlation for quartzite with a coefficient of determination (R^2) = 0.90 is given by

$$DIF = 1.59\ln(\dot{\varepsilon}) - 8.79 \quad \text{for} \quad 553/\text{s} \le \dot{\varepsilon} \le 921/\text{s} \tag{12}$$

The correlation for quartzitic gneiss with a coefficient of determination (R^2) = 0.86 is given by

$$DIF = 1.68\ln(\dot{\varepsilon}) - 8.43 \quad \text{for} \quad 323/\text{s} \le \dot{\varepsilon} \le 985/\text{s} \tag{13}$$

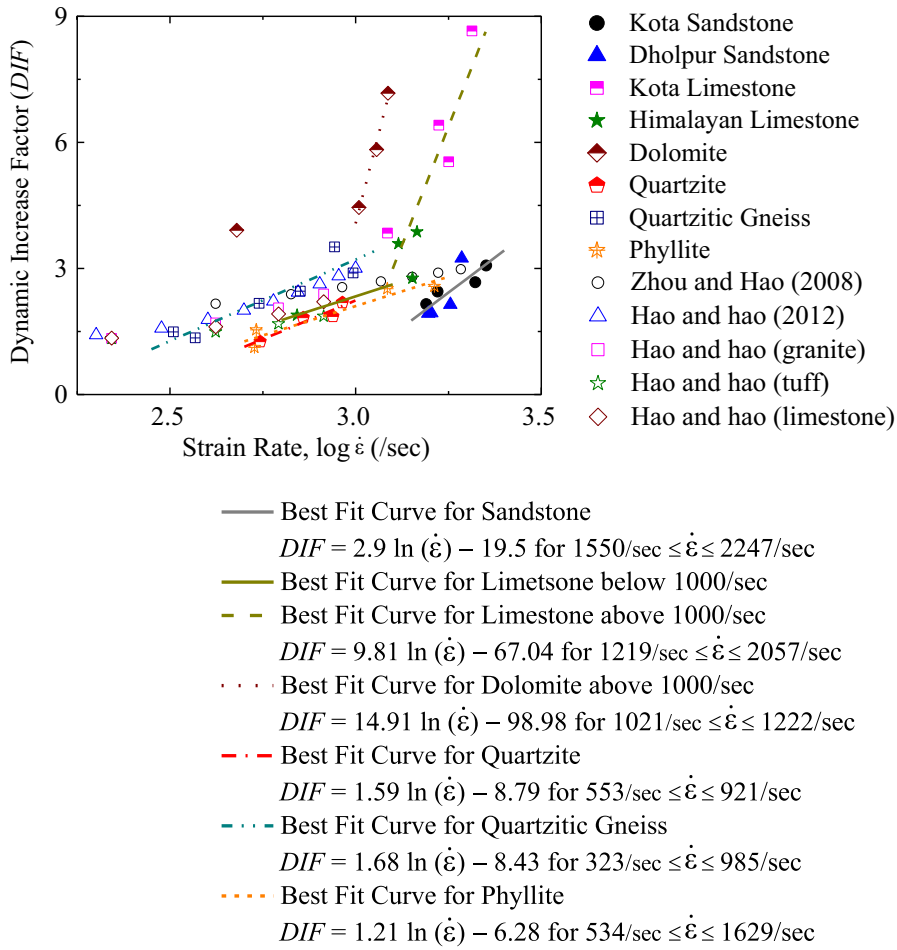

Fig. 14 Best fit *DIF* curve for rocks

The correlation for quartzitic gneiss with a coefficient of determination (R^2) = 0.91 is given by

$$DIF = 1.21\ln(\dot{\varepsilon}) - 6.28 \quad \text{for} \quad 534/\text{s} \le \dot{\varepsilon} \le 1629/\text{s} \tag{14}$$

It may be noted that the *DIF* equation will be applicable for the strain rate range considered in the current work. Figure 14 also compares the proposed *DIF* equation with the previously proposed equations by various researchers. The proposed equation compares well with those obtained from the literature.

6 Conclusions

High strain rate characterization of Kota sandstone, Dholpur sandstone, Kota limestone, Himalayan limestone, dolomite, quartzite, quartzitic gneiss and phyllite has been carried out in the present work for a strain rate range varying from 300 to 2500/s through the compression SHPB test. The physical properties and static stress–strain behavior of the rocks have also been studied. The following conclusions are drawn from the tests.

(1) For Kota sandstone, the peak stress increases at a rate of 13–14% till the strain rate of 1800/s, however, it increases abruptly by 25–45% above 1800/s strain rate. The dynamic stress of the rocks increases rapidly with an increase in the loading rate from quasi-static to dynamic.

(2) For Dholpur sandstone, the peak stress increases slowly at a rate of almost 10% with increasing strain rate up to a strain rate of 1800/s while above 1800/s strain rate, it increases abruptly by 51.47%.

(3) For Kota limestone, the peak stress increases by 55–70% with each increase in strain rate.
(4) For Himalayan limestone, the peak stress increases by 30–80% with each increase in strain rate.
(5) For dolomite, the peak stress increases by 15–30% with each increase in strain rate.
(6) For quartzite, the peak stress increases by 45% with an increase in strain rate from 553 to 723/s strain rate whereas it increases at a very low rate of 1.5% with an increase from 723 to 869/s. The peak stress increases by 17% when the strain rate increases from 869 to 921/s.
(7) For quartzitic gneiss, the peak stress increases by 45–60% with each increase in strain rate.
(8) For phyllite, the peak stress increases by 38–63% with each increase in strain rate.

Acknowledgements Funding was provided by Defence Research and Development Organisation (Grant No. ARMREB/CDSW/2013/151).

References

Akram M, Bakar MZA (2007) Correlation between uniaxial compressive strength and point load index for salt-range rocks. Pak J Eng Appl Sci 1(50):1–8

Alam MS, Chakraborty T, Matsagar V, Rao KS, Sharma P, Singh M (2015) Characterization of Kota sandstone under different strain rates in uniaxial loading. Geotech Geol Eng 33(1):143–152

Anuradha, Mishra S, Chakraborty T, Matsagar V, Chandel P, Singh M (2016) High Strain rate response of himalayan quartzitic gneiss by using split Hopkinson pressure bar. In: Rock dynamics: from research to engineering—2nd international conference on rock dynamics and applications, ROCDYN 2016, pp 93–98

ASTM D4543-08 (2008) Standard practices for preparing rock core as cylindrical test specimens and verifying conformance to dimensional and shape tolerances. American Society for Testing and Materials International, West Conshohocken

ASTM D5731-08 (2008) Standard test method for determination of the point load strength index of rock and application to rock strength classifications. American Society for Testing and Materials International, West Conshohocken

ASTM D7012-14 (2014) Standard test methods for compressive strength and elastic moduli of intact rock core specimens under varying states of stress and temperatures. American Society for Testing and Materials International, West Conshohocken

ASTM E4-16 (2016) Practices for force verification of testing machines. American Society for Testing and Materials International, West Conshohocken

Blanton TL (1981) Effect of Strain Rates from 10^{-2} to 10 sec^{-1} in triaxial compression tests on three rocks. Int J Rock Mech Min Sci Geomech Abstr 18(1):47–62

Chakraborty T, Mishra S, Loukus J, Halonen B, Bekkala B (2016) Characterization of three himalayan rocks using a split hopkinson pressure bar. Int J Rock Mech Min Sci 85:112–118

Chen W, Ravichandran G (1996) An experimental technique for imposing dynamic multiaxial-compression with mechanical confinement. Exp Mech 36:155–158

Chen W, Ravichandran G (2000) Failure mode transition in ceramics under dynamic multiaxial compression. Int J Fract 101:141–159

Christensen RJ, Swanson SR, Brown WS (1972) Split Hopkinson bar tests on rock under confining pressure. Exp Mech 12:508–541

Dai F, Xia KW, Tang LZ (2010) Rate of dependence of the flexural tensile strength of Laurentian granite. Int J Rock Mech Min Sci 47:469–475

Davis EDH, Hunter SC (1963) The dynamic compression testing of solids by the method of the split Hopkinson bar. J Mech Phys Solids 11:155–179

Dusenberry DO (2010) Handbook for blast resistant design of buildings, 1st edn. Wiley, Hoboken, p 512

Field JE, Walley SM, Proud WG, Goldrein HT, Siviour CR (2004) Review of experimental techniques for high rate deformation and shock studies. Int J Impact Eng 30(7):725–775

Frew DJ, Forrestal MJ, Chen W (2001) A split Hopkinson pressure bar technique to determine compressive stress–strain data for rock materials. Exp Mech 41(1):40–46

Fukui K, Okubo S, Ogawa A (2004) Some Aspects of loading-rate dependency of Sanjome andesite strengths. Int J Rock Mech Min Sci 41(7):1215–1219

Gray G (2000) Classic split-Hopkinson pressure bar testing. In: Kuhn H, Medlin D (eds) American society of metals handbook, mechanical testing and evaluation, vol 8. ASM International, Novelty, pp 1027–1094

Hao Y, Hao H (2012) Numerical investigation of the dynamic compressive behaviour of rock materials at high strain rate. Rock Mech Rock Eng 46(2):373–388

ISRM (1985) International Society of Rock Mechanics Commission on testing methods, suggested method for determining point load strength. Int J Rock Mech Min Sci Geomech Abstr 22:51–60

Klepaczko JR (1990) Behavior of rock-like materials at high strain rates in compression. Int J Plast 6:415–432

Kolsky H (1949) An investigation of the mechanical properties of materials at very high rates of loading. Proc R Soc A Math Phys Eng Sci B62:676–700

Kolsky H (1953) Stress waves in solids. Clarendon Press, Oxford

Kumar R (2007) Testing and constitutive modelling of the strain-softening behaviour of some rocks. Ph.D. Thesis, Indian Institute of Technology (IIT) Delhi

Li QM, Meng H (2003) About the dynamic strength enhancement of concrete-like materials in a split Hopkinson pressure bar test. Int J Solids Struct 40(2):343–360

Lindholm US, Yeakley LM, Nagy A (1974) The dynamic strength and fracture properties of Dresser basalt. Int J Rock Mech Min Sci Geomech Abstr 11:181–191

Lu YB, Li QM, Ma GW (2010) Numerical investigation of the dynamic compressive strength of rocks based on split Hopkinson pressure bar tests. Int J Rock Mech Min Sci 47(5):829–838

Nemant-Nasser S, Isaacs JB, Starrett JE (1991) Hopkinson techniques for dynamic recovery experiments. Proc R Soc A Math Phys Eng Sci 435:371–391

Ngo T, Mendis P, Gupta A, Ramsay J (2007) Blast loading and blast effects on structures—an overview. Electron J Struct Eng Spec Issue Load Struct 7:76–91

Olsson WA (1991) The compressive strength of tuff as a function of strain rate from 10^{-6} to 10^{3}/s. Int J Rock Mech Min Sci Geomech Abstr 28(1):115–118

Perkins RD, Green SJ (1970) Uniaxial stress behavior of porphyritic tonalite at strain rates to 10^{3}/second. Int J Rock Mech Min Sci 7:527–535

Ravichandran G, Subhash G (1994) Critical appraisal of limiting strain rates for compression testing of ceramics in a split Hopkinson pressure bar. J Am Ceram Soc 77:263–267

Ross CA, Thompson PY, Tedesco JW (1989) Split Hopkinson pressure-bar tests on concrete and mortar in tension and compression. ACI Mater J 86:475–481

Ross CA, Tedesco JW, Kuennen ST (1995) Effects of strain-rate on concrete strength. ACI Mater J 92:37–47

Sarva S, Nemat-Nasser S (2001) Dynamic compressive strength of silicon carbide under uniaxial compression. Mater Sci Eng 317:140–144

Singh M, Sood D, Gupta RK, Kumar R, Gautam PC, Sewak B, Sharma AC, Mathew T (2008) Dynamic yield strength of mild steel under impact loading. Def Sci J 58(2):275–284

Tyrell GW (1978) The principles of petrology: an introduction to the science of rocks. Springer, Berlin

Veyera GE, Ross CA (1995) High strain rate testing of unsaturated sands using a split-Hopkinson pressure bar. In: Proceedings of 3rd international conference on recent advances in geotechnical earthquake engineering and soil dynamics, St-Louis, USA, pp 31–34

Xia K, Yao W (2015) Dynamic rock tests using split Hopkinson (Kolsky) bar system—a review. J Rock Mech Geotech Eng 7:27–59

Xia K, Nasseri MHB, Mohanty B, Lu F, Chen R, Luo SN (2008) Effects of microstructures on dynamic compression of barre granite. Int J Rock Mech Min Sci 45:879–887

Zhang W, Hao P, Liu Y, Shu X (2011) Determination of the dynamic response of Q345 steel materials by using SHPB. Procedia Eng 24:773–777

Zhou XQ, Hao H (2008) Modelling of compressive behaviour of concrete-like materials at high strain rate. Int J Solids Struct 45(17):4648–4661

Zhou Y, Zhao J (2011) Advances in rock dynamics and applications. CRC Press, Taylor and Francis Group, Boca Raton

Zhou YX, Xia K, Li XB, Li HB, Ma GW, Zhao J, Zhou ZL, Dai F (2011) Suggested methods for determining the dynamic strength parameters and mode-i fracture toughness of rock materials. In: The ISRM (International Society of Rock Mechanics) suggested methods for rock characterization, testing, and monitoring: 2007–2014, International Society for Rock Mechanics Commission on testing methods

Zhu WC, Bai Y, Li XB, Niu LL (2012) Numerical simulation on rock failure under combined static and dynamic loading during SHPB tests. Int J Impact Eng 49:142–157